Properties of Tornado Wind Speed Profiles Used in the Development of the ASCE 7-22 Tornado Provisions

Franklin T. Lombardo, A.M.ASCE[1]; Zachary B. Wienhoff[2]; Maryam Refan[3]; Joshua Wurman[4]; Karen Kosiba[5]; and Marc Levitan, F.ASCE[6]

Abstract: Significant tornado events have prompted a push for the development of design standards that consider tornado loading for conventional buildings and structures. One important loading parameter in the design standards is the variation in the horizontal wind speed with the height (i.e., wind speed profile) as manifested in a velocity pressure profile. Different from the atmospheric boundary layer (ABL) in which the wind speed monotonically increases with height, the average wind speed profile in tornadoes exhibits a "nose-like" profile for which the wind speed increases from the surface to a local maximum at "nose" height and then decreases above that height. A tornado task committee (TTC) was convened through the ASCE 7 Wind Load Subcommittee, in part to report on the collection, review, and analysis of tornado wind speed profile data and to propose a "design" tornado velocity pressure profile for inclusion in the new tornado load chapter of the ASCE 7-22 standard. A total of 36 tornado profiles were evaluated independent of terrain exposure or surface roughness and collected from mobile radar data. Significant variability was noted in the profiles, but many showed a peak horizontal wind speed relatively close to surface, with a median height of approximately 164 ft (50 m). A proposed tornado velocity pressure profile and associated velocity pressure exposure coefficient, K_{zTor}, was then developed for ASCE 7-22. The proposed nominal tornado profile closely followed the median radar profile. Values of the new $K_{zTor} = 1.0$ between ground level and 200 ft (61 m) decrease linearly to 0.9 at a height of 328 ft (100 m) then remain constant above that height. **DOI: 10.1061/JSENDH.STENG-12625.**

Introduction

Significant tornado events in the recent past have prompted a push for the development of design standards that consider tornado loading for conventional buildings and structures, which have not previously been designed for tornado hazards (FEMA 2012; NIST 2014). Considering tornadoes in the design of structures requires a reassessment of the parameters currently used in wind load design (e.g., tornadic wind speed) and a new assessment of parameters not currently considered (e.g., atmospheric pressure change). Because full-scale tornado loading data do not exist and field measurements of wind speed are few, a number of researchers have turned to numerical simulations (e.g., Hu et al. 2011; Cao et al. 2018; Yuan et al. 2019) or wind tunnel testing (e.g., Haan et al. 2010; Refan and Hangan 2016; Gillmeier et al. 2018) to generate these parameters.

One of the more important wind loading parameters is the variation in the horizontal wind speed with height (i.e., wind speed profile). It is assumed in most codes and standards that the behavior of this wind speed profile is monotonically increasing due to the influence of surface friction, i.e., atmospheric boundary layer (ABL) profile with height. The ABL profile is correlated with the velocity pressure profile (which is a function of the square of the wind speed profile) on the windward face of the building, signifying that wind loading also increases with height. In the ASCE 7 standard (ASCE 2022), this profile is given the variable designation K_z and includes different profile shapes as a function of surface roughness. The profile shape is also associated with different wind load distributions around a bluff body. For example a more uniform wind profile leads to a more uniform pressure profile on the roof, whereas a more sheared profile is favorable for higher suction on the roof edge (Jensen 1958; Cook 1986).

Information on tornado wind speed profiles is scattered across the literature in various forms, usually in studies in which the profile was not the primary focus. From theoretical (e.g., Kuo 1971) and wind tunnel (e.g., Church et al. 1977; Refan and Hangan 2018; Tang et al. 2018) models, as well as the limited field data that exist (e.g., Wurman et al. 2007; Kosiba and Wurman 2013, 2023), significant differences have been noted from an ABL profile. More specifically, a "nose" has been noted in the profile in which the wind speed increases from the surface to an overall maximum at a "nose" height and then decreases above that height. Physically, the nose is likely the result of the conservation of momentum in the tornado. As the tornado wind field interacts with the rough surface, the flow turns toward the low pressure center (i.e., tornado center) as frictional forces increase, initiating a reduction in the tornado core radius that causes the near-surface wind field to accelerate. However, friction still slows down the flow right near the surface, causing a maximum at some height above the surface (Davies-Jones et al. 2001). Wind tunnel and numerical simulations suggest that this nose is generally more pronounced near the radius of

[1]Associate Professor, Dept. of Civil and Environmental Engineering, Univ. of Illinois at Urbana-Champaign, 205 N. Mathews Ave., Urbana, IL 61801 (corresponding author). ORCID: https://orcid.org/0009-0005-7759-5078. Email: lombaf@illinois.edu

[2]Convective Storms Analyst, State Farm, 1 State Farm Plaza, Bloomington, IL 61791. Email: wienhof1@gmail.com

[3]Operations Leader, CPP Wind Engineering, 2655 North Sheridan Way, Suite 290, Mississauga, ON, Canada L5K 2P8. Email: mrefan@cppwind.com

[4]Executive Director, FARM Facility, Univ. of Alabama in Huntsville, Huntsville, AL 35899. Email: jwurman@uah.edu

[5]Managing Director, FARM Facility, Univ. of Alabama in Huntsville, Huntsville, AL 35899. Email: kakosiba@uah.edu

[6]Lead Research Engineer, National Windstorm Impact Reduction Program, National Institute of Standards and Technology, 200 Bureau Dr., Gaithersburg, MD 20877. Email: marc.levitan@nist.gov

Note. This manuscript was submitted on March 27, 2023; approved on June 21, 2024; published online on October 22, 2024. Discussion period open until March 22, 2025; separate discussions must be submitted for individual papers. This paper is part of the ***Journal of Structural Engineering***, © ASCE, ISSN 0733-9445.

maximum wind (RMW), decreasing with increasing distance from the RMW (Refan and Hangan 2018).

When discussing the wind flow pertaining to a tornado and the associated wind profile, it is usually separated into three orthogonal velocity components. For engineering models, these components are generally defined as radial—toward or away from the tornado center—tangential—perpendicular to the radial flow—and vertical—either upward or downward. The definitions of these components have different meanings depending on the context, as is subsequently discussed. The maximum wind speed relatively close to the surface (i.e., nose) is observed in the tangential and radial components near the RMW, as illustrated in Fig. 1. The profiles in Fig. 1 are based on one realization of an analytical tornado vortex model from Wen (1975) based on Kuo (1971). The RMW has generally been the location of the maximum tangential wind speed in the tornado but has been defined in other publications (Wood and Brown 2011) as the location of the maximum horizontal speed (vector sum of radial and tangential). Although the vertical component can be significant in tornadoes, given the limitations in measuring this quantity and the incorporation of this component through the pressure coefficient values in tornado loading through ASCE 7-22, it is not discussed in this study.

A tornado task committee (TTC) was convened in 2018 through the ASCE 7 Wind Load Subcommittee with the purpose of developing criteria for tornado loads on buildings and other structures. Much of the TTC work addressed the determination and quantification of the parameters important to tornado loading. The focus of this paper is to report on the collection, review, and analysis of tornado wind speed profile data from several sources and to document the development of the "design" tornado velocity pressure profile (K_{zTor}, where Tor = tornado), which was incorporated in the new Chapter 32: Tornado Loads in ASCE 7-22 (ASCE 2022). The decision was made to use the 36 radar profiles at the time of ground-relative maximum intensity (i.e., radar-maximum data) as the primary basis for the proposed ASCE 7 loading profile. This choice was made for several reasons. Although numerical and experimental profiles were initially considered, they are idealized as representing a specific set of conditions, such as terrain, tornado intensity, and tornado structure. In addition, the radar-maximum profiles were judged to more closely represent a "design" event (i.e., similar to a short duration gust) with no significant spatial and/or temporal averaging. In ASCE 7, this choice also has a link to ABL winds, the models of which were also partially based on field collected data through Harris and Deaves (1980) and from large-eddy simulations outlined in Kelly et al. (2019). An additional discussion on the K_z profiles for the ABL used in ASCE 7-22 can be found in Yeo et al. (2023). A further rationale behind the proposed profile for ASCE 7 tornado loads is discussed in the next section.

The sections of this paper cover, in order, the collection of tornado profiles and their characteristics; analysis of the profiles; the choice of a design profile for ASCE 7; and finally, conclusions.

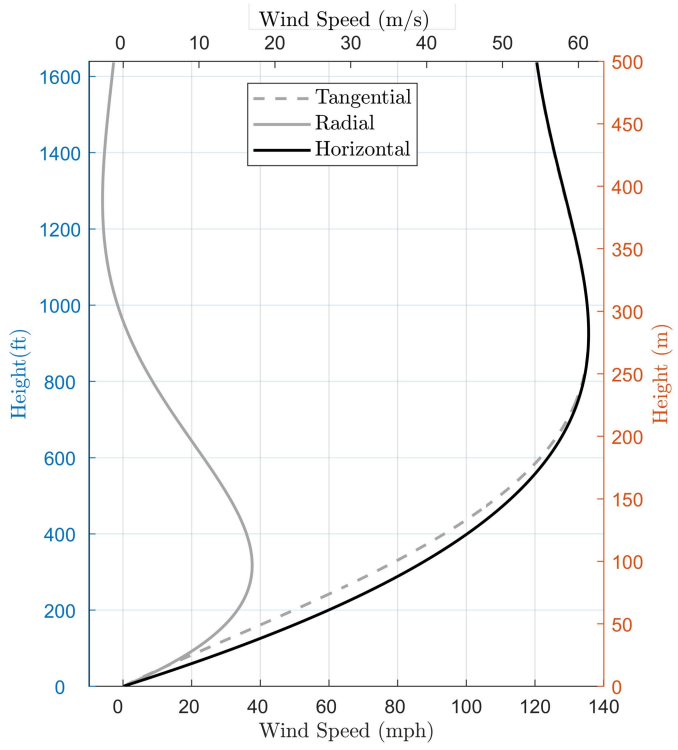

Fig. 1. Radial and tangential tornado velocity profiles and total horizontal wind speed profile near RMW using equations from Wen (1975). "Negative" velocity for radial component is directed away from the pressure gradient.

Tornado Wind Speed Profile Data Collection and Characteristics

The radar measurements in this study were collected using a fleet of Doppler on Wheels (DOW) mobile radars (Wurman et al. 2021b). One important caveat of radar measurements is that they are *not* point measurements. Although the Doppler velocity sampled by the radar is effectively instantaneous in time (integration times are typically $\ll$1 s), *it is a returned power-weighted volumetric average of the component of the mean velocity toward or away from the radar.* The volume over which this average is calculated increases with distance from the radar because of radar beam spreading. At close ranges to tornadoes, the linear dimensions of the radar volumes may be smaller than the time-space converted linear dimension of point in situ anemometer measurements using typical averaging times. For example, at a 2-km (1.2-mi) range to a tornado, a radar volume might be approximately $30 \times 30 \times 12$ m ($100 \times 100 \times 40$ ft). At typical tornado wind speeds of approximately 135 mph (60 m/s), air moves through this volume in ~0.5 s.

A detailed analysis of DOW-derived tornado properties at their time of maximum intensity for 120 tornadoes observed between 1995 and 2006 is found in Wurman et al. (2021a). A detailed analysis of vertical profiles of the horizontal winds in 73 tornadoes of varying intensity at their time of maximum intensity, observed between 1995 and 2009, is found in Kosiba and Wurman (2023). In the current study, DOW radar-derived vertical profiles were extracted for 36 tornado profiles from the preliminary database of 120 DOW observations of many tornadoes at close range (Wurman et al. 2021a) and are used to construct tornado wind profiles at their observed time and location of maximum wind intensity (i.e., approximately at the RMW). The vertical profiles represent ground-relative horizontal velocities, which have been calculated using Doppler wind measurements, corrections for smoothing due to coarse spatial sampling, and the unobserved component of tornadoes' vector wind fields. The propagation speed was calculated from the location of the tornado centers observed in subsequent near-ground radar sweeps. An application of this method can be found in Wurman et al. (2021a). Profiles are selected at the time of the maximum observed ground-relative wind intensity and may not be the time of actual maximum intensity since the tornado may not have been observed

at the time of maximum intensity. Measurements represent "snapshots" of quasi-horizontal wind speeds ("quasi" because the radar beams are usually slightly inclined to the ground, making the measured Doppler velocity component not exactly horizontal) at each observation height collected over a radar sample volume. Altitudes in the profiles represent the height above the ground at the radar and have not been corrected for differences in altitude between the radar and the location of the measurements. Tornadoes exhibit a wide range of structures (Wurman and Kosiba 2013), in many cases deviating substantially from the simple axisymmetric structure assumed when corrections for observing geometry and vortex motion were made (e.g., multiple vortex structure; Wurman 2002; Alexander and Wurman 2005; Wurman et al. 2014). These affect the interpretation and representativeness of individual profiles, whereas the overall statistics remain valid. Finally, the tornado structure is often very transient, and snapshots of vertical profiles can vary greatly from time to time (e.g., Kosiba and Wurman 2013); the profiles used herein represent snapshots from the radar scanning volumes at the time of maximum observed intensity, and their representativeness of tornado structure at other times is not yet known. This set of 36 tornado profiles was extracted from tornadoes with maximum ground-relative radial velocities (V_{max}) ranging from 61 mph (27.3 m/s) to 304 mph (136 m/s) with a median value of 121 mph (54.3 m/s). These tornadoes and subsequent tornado profiles were generated from tornadoes spawned from supercell thunderstorm mesocyclones (Wurman et al. 2021a). Supercells are responsible for a majority of tornado reports (Ashley et al. 2019) and have produced the strongest tornadoes. It is acknowledged that the profiles analyzed here represent a small subset of tornadoes and associated profiles. Where these tornado profiles fit within the larger population is unknown. These profiles are referred to as the radar-maximum measurements in this paper.

In the process of determining design tornado velocity pressure profiles, a number of other references were consulted, as previously mentioned. These references included an analysis of azimuthally averaged radar data (e.g., Kosiba and Wurman 2013; Refan et al. 2017; Wurman et al. 2021a; Kosiba and Wurman 2023) using the ground-based velocity track display (GBVTD) technique (e.g., Lee et al. 1999; Lee and Wurman 2005; Kosiba and Wurman 2010), wind tunnel data (e.g., Zhang and Sarkar 2012; Refan et al. 2014; Refan and Hangan 2018; Tang et al. 2018; Wang et al. 2017) and numerical studies (e.g., Nolan et al. 2017; Reinhart et al. 2018; Dahl et al. 2017). Although not explicitly used in the development of the ASCE 7-22 profile, profiles from these studies were used in an initial comparison of the radar data. More rigorous comparisons were not performed due to the difficulty or perhaps impossibility of 1:1 comparisons with the radar data due to, for example, the boundary conditions of the numerical simulations, characteristics of the particular wind tunnel, and the nonuniformity of the characteristics between the experiments and simulations. Information from the simulations could be used to supplement and enhance the chosen tornado velocity pressure profile in subsequent versions.

Tornado Wind Speed Profile Assumptions and Limitations

Averaging Time

Concepts such as averaging time are not standardized and/or straightforward, as alluded to in the radar data discussion; therefore, no specific averaging time is reflected in the profiles analyzed in this study.

Exposure

Radar deployments were partial toward open, flat terrain. Most available research has suggested that tornado characteristics are modified by exposure, which includes topographic effects, and these modifications are greatest near the ground. However, substantial challenges exist in providing general guidance in how topographic effects modulate tornado characteristics. Given the need to increase the wealth of realistic exposures in experiments to provide better guidance, no modifications for exposure were made. The Commentary section in ASCE 7-22 associated with tornado loading contains information on tornado intensity and structure changes with exposure.

Tornado Structure

Swirl ratio, a nondimensional ratio of the angular to radial momentum, is an important parameter for ascertaining tornado structure, and its value depends on the flow characteristics of the vortex (Church et al. 1977). Any analysis dependent on the swirl ratio could not be done because of the averaging techniques employed, and the difficulty in assessing the swirl ratio in the field (Kosiba and Wurman 2013).

Normalized Wind Profile

To better reflect the behavior of profiles of tornadoes close to the ground, i.e., relevant to the overwhelming majority of buildings and other structures, only radar-maximum profiles that had a minimum observation height below 198 ft (60 m) were kept for analysis. This condition left 36 profiles for analysis.

To provide consistency with the velocity pressure exposure coefficient (K_z) used in ASCE 7 for nontornadic wind hazards, the first step was to normalize the profiles using a speed at a given height. To visualize at which height the maximum wind speed occurred in the profiles (z_{max}), each profile was normalized by its maximum wind speed (V_{max}) at z_{max}. This normalization is illustrated in Fig. 2 for all 36 tornado profiles in the lowest 1,640 ft (500 m). Fig. 2 shows that z_{max} is lower than 330 ft (100 m) for a majority of cases (~67%) with a median z_{max} of approximately 156 ft (47.5 m). A linear interpolation was assumed between measurement heights in the profiles.

The complete set of profiles was then normalized by the wind speed at the *closest* observation height of 164 ft (50 m), denoted as V_{50}. The 164 ft (50 m) normalization was chosen for its proximity to the median z_{max} and the corresponding significance of the "nose" location at that height. It should be noted that the character of the normalized profile is sensitive to the minimum height of the data collected. Fig. 3 shows the results of the normalization for all 36 individual profiles in the lowest 1,640 ft (500 m).

Figs. 2 and 3 show significant variability in the profiles. A similar variability has been noted in profiles generated from thunderstorms (Lombardo et al. 2014). To obtain a more detailed look near the surface, Fig. 4 displays the profiles in the lowest 500 ft (150 m) in log scale. Some of the radar-maximum profiles displayed an overall peak closest to the surface, which has been shown in Kosiba and Wurman (2013, 2023). Fig. 4 is especially helpful for elucidating the lack of measurements right near the ground, especially in the lowest 33 ft (10 m).

Measures of the central tendency of the profiles were calculated. Given the significant variability in the normalized profile data point values, the median value (instead of the mean) was used as a central tendency measure to reduce the effects of outliers. To create median profiles, the measurements were binned in height ranges of 66 ft

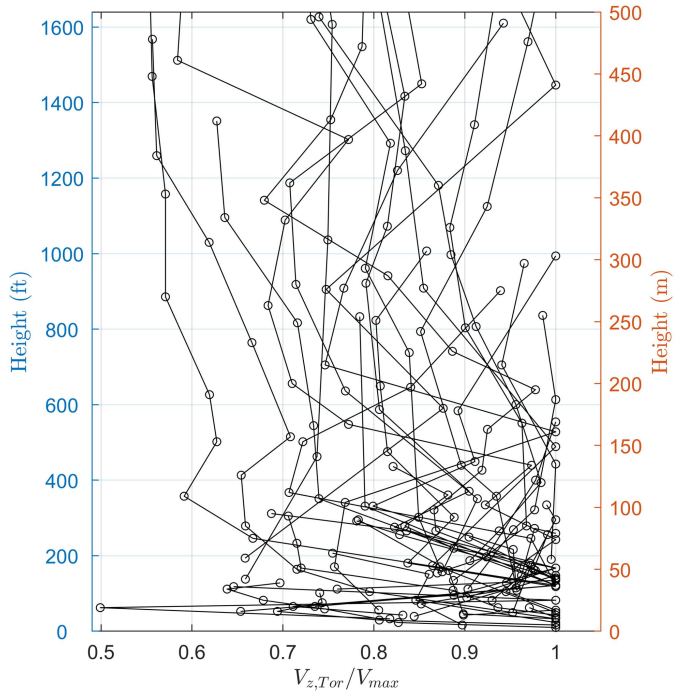

Fig. 2. All 36 tornado wind speed profiles normalized by its corresponding $V_{\max}$.

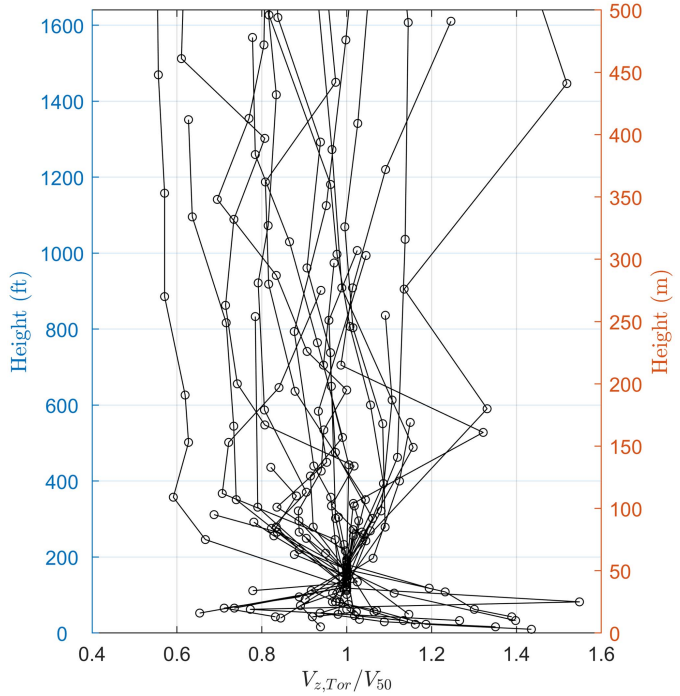

Fig. 3. Tornado wind speed profiles normalized by V_{50}.

(20 m) up to a height of 328 ft (100 m) and in ranges of 164 ft (50 m) above 328 ft (100 m) to minimize large variations that could be present in smaller bins. If at least 10 observations were found to be in each bin, the median and standard deviation of the normalized profile data point values were calculated. If less than 10 observations were found in a bin, the height of the bin was extended by one bin height, 66 ft (20 m) or 164 ft (50 m) depending on the height, until the condition was met. The standard deviation of the normalized

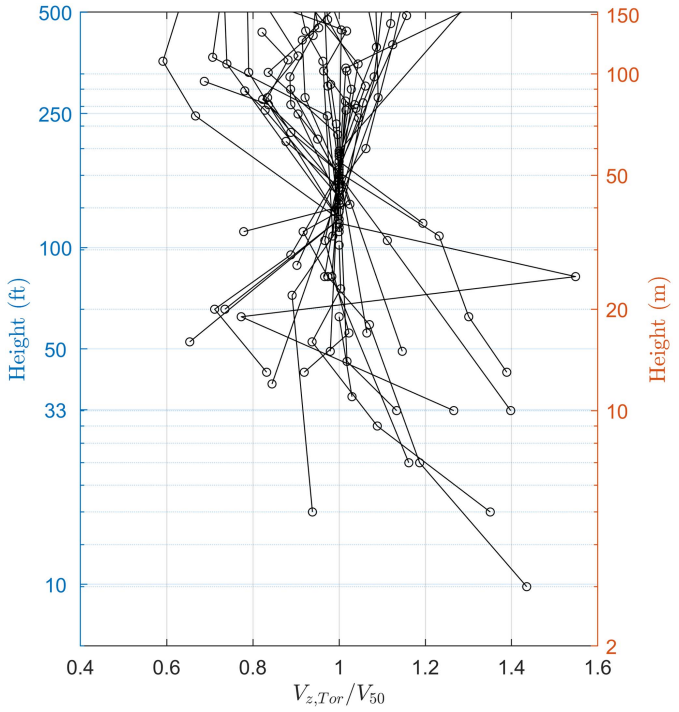

Fig. 4. Detailed view of normalized profiles from Fig. 3 showing lowest 500 ft (150 m) of measurements, with height plotted on log scale.

profile values was also calculated for a discussion on the development of the tornado velocity pressure profile (next section).

Development of the Tornadic Velocity Pressure Profile

The goal was then to determine an appropriate tornado velocity pressure profile given the available radar (maximum) data analyzed in the previous section for ASCE 7. Within the ASCE 7 wind loading framework, the design (i.e., basic) wind speed is defined as a 3-s gust speed at 33 ft (10 m) over flat open terrain. The variation in wind speed with a height above ground and exposure conditions (based on upwind surface roughness) is handled through the velocity pressure exposure coefficient, K_z. This coefficient is effectively equal to the square of a normalized ABL peak gust wind speed profile, where the normalization height is 33 ft (10 m) [Eq. (1)]. V_{10} is the 33 ft (10 m) wind speed in "open" terrain (Exposure C), and V is the wind speed at a specific height and in a specific exposure. To propose a tornado velocity pressure profile in the ASCE 7 standard (similar to K_z), the transition needs to be made from a wind speed profile to a velocity pressure profile, resulting in a new tornado velocity pressure exposure coefficient, K_{zTor} [Eq. (2)], where $V_{z,Tor}/V_{50}$ is the normalization shown in Figs. 3–5. It should be reiterated that Eq. (1) is for ABL profiles, and Eq. (2) is for the radar maximum profiles discussed in this paper. The K_{zTor} profiles were developed independent of terrain effects, which is not the case for K_z

$$K_z = \left(\frac{V}{V_{10}}\right)^2 \tag{1}$$

$$K_{zTor} = \left(\frac{V_{z,Tor}}{V_{50}}\right)^2 \tag{2}$$

The results of this analysis are shown in Fig. 5, where the median binned values for all are plotted at midbin height overlaid on the individual radar profiles originally shown in Fig. 3. The radar data can be observed to exhibit a slight decrease in speed above the normalization height using the median binned values. The radar maximum set has a near constant median value of approximately 0.95 up to approximately 1,000 ft (300 m). Below the normalization height, the radar maximum profiles remaining very near 1.0 or slightly greater, exhibiting an increase to the lowest bin-averaged height (33 ft, 10 m) of approximately 6% (1.06).

Fig. 5 shows all 36 normalized radar-maximum profiles and the median and median plus and minus one standard deviation profiles using the binned ranges described in the Normalized Wind Profile Analysis section. The normalized profiles are now labeled as $\sqrt{K_{zTor}}$ to show consistency with Eq. (2). Above the bin centered at 1,312 ft (400 m), not a sufficient number of measurements existed to create another bin to continue the median profile.

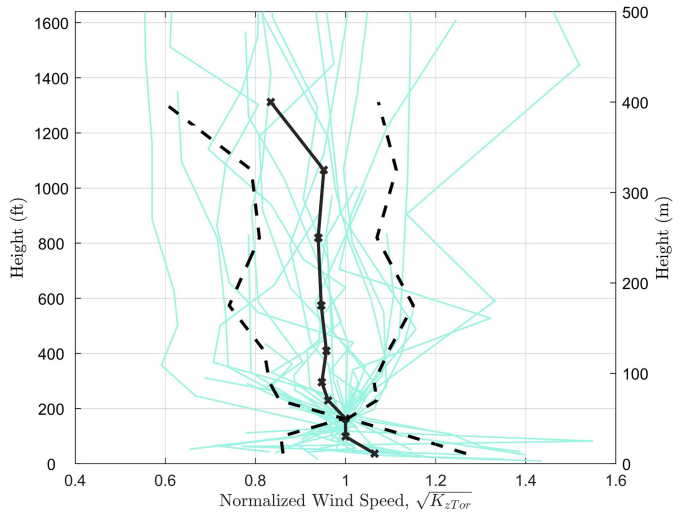

Fig. 5. Normalized radar profiles. Median profile for all measurements (solid), median plus and minus one standard deviation of all profiles (dashed), and individual profiles.

As previously noted and shown in Fig. 5, a significant amount of variability existed in the radar maximum profiles. Standard deviations of $\sqrt{K_{zTor}}$ values away from the normalization height ranged from 0.11 to 0.23. A closer look at the distribution of $\sqrt{K_{zTor}}$ values for two height ranges reveals that the distributions are skewed (i.e., nonsymmetric). As may be expected given that the median height of the nose was approximately 164 ft (50 m), the most common $\sqrt{K_{zTor}}$ value for both plots is approximately 1.0. Between 164 ft (50 m) and 328 ft (100 m), the distribution is skewed to values less than 1.0 and is skewed to values greater than 1.0 below 50 m. These results suggest that the wind speed does tend to decrease above 164 ft (50 m).

Fig. 6 also shows that the variability in the normalized profile data points decreases with increasing height. In other words, the profiles show higher uncertainty near the ground. The standard deviations for $\sqrt{K_{zTor}}$ in the height ranges below and above 164 ft (50 m) are 0.16 and 0.10, respectively. The opposite trend holds true for skewness values of 0.83 and –1.2 for lower and upper height ranges, respectively. It should be noted that the variability in $\sqrt{K_{zTor}}$ is sensitive to the minimum observation height and the specific normalization height. The variability in the profiles was not used in the proposed design profile subsequently discussed in this paper. However, the variability was accounted for in the full reliability analysis (Li et al. 2024) conducted to determine the appropriate return periods for the tornado hazard maps in ASCE 7-22 (ASCE 2022), adapting the reliability methods used for other wind hazards (McAllister et al. 2018).

The nominal tornado speed profile ($\sqrt{K_{zTor}}$) developed for ASCE 7 closely follows the median profile for all radar-maximum measurements, as shown in Fig. 7. A constant $\sqrt{K_{zTor}}$ profile value of 1.0 was selected for all heights below 200 ft (61 m). Although the normalized median profile value for the lowest bin at a 33-ft (10-m) height had a slightly greater value (1.06), the ASCE 7 profile was set to 1.0 in that region as well. The slight profile value increase above 1.0 is driven by the very few radar data points below 33 ft (10 m). Given the limited data and large variability (e.g., and the uncertain effects of terrain and topography, which were not accounted for in ASCE 7-22), extending the 1.0 normalized profile

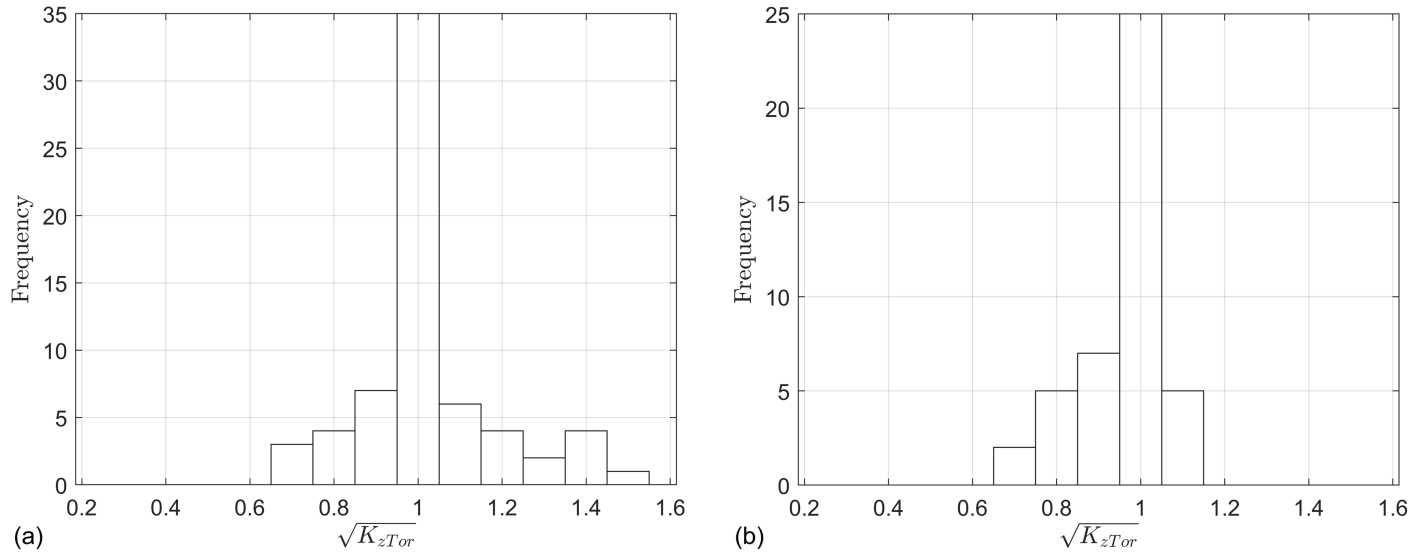

Fig. 6. Distribution of normalized profile data point values for two height ranges: (a) 0–164 ft (0–50 m); and (b) 164–328 ft (50–100 m) for radar maximum profiles.

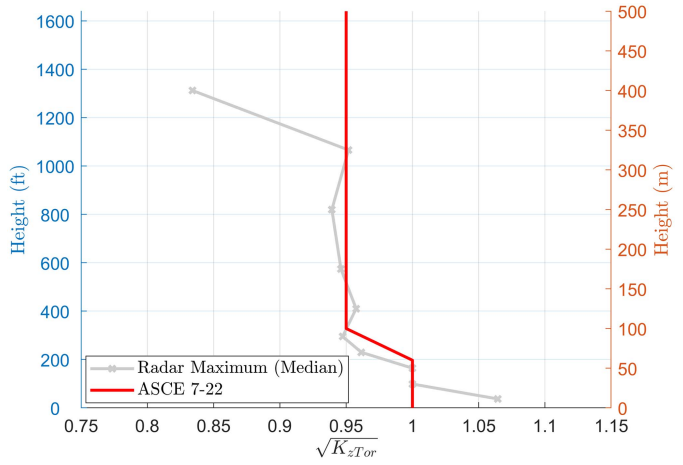

Fig. 7. Median radar maximum profile compared with $\sqrt{K_{zTor}}$ values for ASCE 7-22.

value all the way to the ground made sense. Between 200 ft (61 m) and 328 ft (100 m), a linear function was used to represent the slight tapering off behavior apparent in the median profile. Above 328 ft (100 m), the profile was kept at 0.95 because the median profile tended to stabilize around that value as the height increased. Above approximately 1,066 ft (325 m), the median radar profile decreased slightly; however, given the lack of data, which necessitated increasing the bin size and the substantial uncertainty, the profile value was conservatively maintained at 0.95 above this height. In practice, this will have little to no impact because (1) extremely few buildings and other structures are that tall, and (2) tornado loads are unlikely to have control over other wind loads at these heights due to the increasing wind speed with height in ABL flows (Fig. 8).

Fig. 8 shows the K_{zTor} profile for tornadoes as compared to the K_z profiles for Exposures B, C, and D from Chapter 26 of ASCE 7-22. Exposure B represents urban, suburban, and wooded upwind terrain, Exposure C is for flat, open terrain, and Exposure D represents marine exposure. Fig. 8 clearly shows that when the K_{zTor} profile is used instead of K_z, assuming that all other loading parameters in ASCE 7 are the same, loading significantly increases for tornadoes closer to the ground, especially for Exposure B and to a lesser extent for Exposure C. This effect is reversed above 33 ft

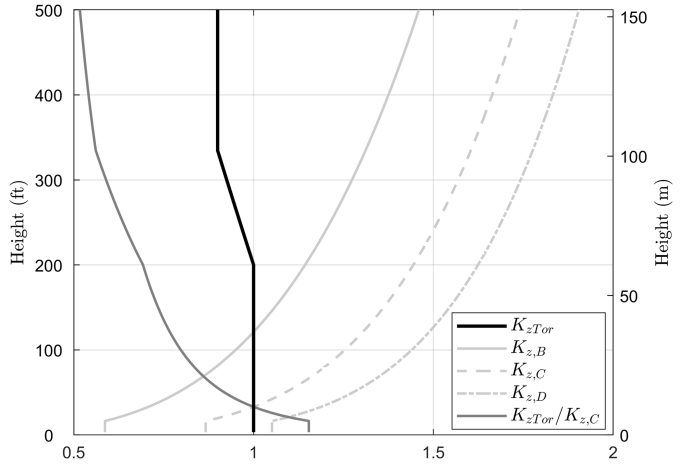

Fig. 8. Velocity pressure exposure coefficient for tornadoes and nontornadoes in ASCE 7-22.

Table 1. Proposed tornado velocity pressure exposure coefficient, K_{zTor} Table for ASCE 7-22

Height above ground level, z		
ft	m	K_{zTor}
0–200	0–61.0	1.0
250	76.2	0.96
300	91.4	0.92
>328	>100	0.90

(10 m) for Exposure C and above approximately 100 ft (30 m) for Exposure B. The ratio between K_{zTor} and K_z for Exposure C illustrates this description in Fig. 8. Tornado loads are less than wind loads for all heights for Exposure D assuming that all other parameters are the same. However, in reality, most of the other proposed loading coefficients for tornadoes *are* different than their nontornadic wind counterparts (ASCE 2022). However, the significant changes between tornado and ABL profiles, as reflected in K_{zTor} versus K_z, are one of the main drivers of the differences between tornado and wind loads when calculating the loads in ASCE 7. The tornado profile shown in Fig. 8 was ultimately approved and included in ASCE 7-22. The tabular form is shown in Table 1, which includes equations in customary and SI units.

The tornado velocity pressure exposure coefficient K_{zTor} can be determined from the following formula:

$$\text{For } 0 < z \le 200 \text{ ft } (61 \text{ m}), \qquad K_{zTor} = 1.0$$

$$\text{For } 200 < z \le 328 \text{ ft}, \quad K_{zTor} = [(2820 - z)/2620]^2, \quad \text{where } z \text{ is in ft}$$

$$\text{For } 61 < z \le 100 \text{ m}, \quad K_{zTor} = [(861 - z)/800]^2, \quad \text{where } z \text{ is in m}$$

$$\text{For } z > 328 \text{ ft}, \qquad (100 \text{ m}) \; K_{zTor} = 0.90$$

Conclusions

As the engineering design of buildings and other structures that incorporate tornado loading becomes more common, especially in the US, it is important to assess the parameters needed for the determination of tornadic wind loads. One of those parameters is the character of the vertical profile of the horizontal wind speed in tornadoes, which has been shown to be significantly different than the ABL profiles currently used in wind loading codes and standards.

A total of 36 tornado profiles assessed near the radius of maximum winds with a minimum observation height lower than 200 ft (61 m) above ground were assessed. These assessments were conducted independent of terrain exposure or surface roughness. The profiles were obtained through field measurements from mobile radar. It was determined that the data set of 36 radar "maximum" profiles are used as the primary basis for the codified tornado load profile due to a closer relationship with the existing profiles in ASCE 7, which are based on field data and represent a gust-like event (i.e., event of a short duration).

The analysis of normalized wind speed profiles revealed significant variability. Despite this variability, many of the profiles showed a peak wind speed relatively close to the surface, with a median peak speed height of approximately 164 ft (50 m). When normalized and binned into height ranges, the median profile shows a reduction in the normalized profile value at elevations greater than the normalization height of 164 ft (50 m). These results, in an averaged sense, support the idea of a "nose" in the profile at heights

relatively close to the ground. A broader and expected conclusion is that tornado wind profiles are significantly different than those of the atmospheric boundary layer.

Based on the wind speed profile analysis, a tornado velocity pressure profile was developed for incorporation into ASCE 7-22 as part of a new chapter on tornado loads. The nominal tornado profile followed closely the median radar profile. A new tornado velocity pressure exposure coefficient, K_{zTor}, was then developed. Similar in format to the existing velocity pressure exposure coefficient (K_z) for nontornadic winds, K_{zTor} is effectively equal to the square of the nominal tornado profile. Values of the new $K_{zTor} = 1.0$ between ground level and 200 ft (61 m), decrease linearly to 0.9 at a height of 328 ft (100 m), then remain constant above that height. The greatest uncertainty in K_{zTor} is in the lowest 33 ft (10 m), where the few radar measurements indicated an increasing trend approaching the ground. K_{zTor} is independent of terrain exposure. It is important to note that radar observations of individual tornadoes (Kosiba and Wurman 2013) and broader samplings over more tornadoes and tornado intensities (Kosiba and Wurman 2023) indicate that the slope of the wind profiles may be typically even more negative than these results indicate, with wind speeds at 328 ft (100 m) above ground level (AGL) averaging near 70% of those at 50 ft (15 m) above ground.

Data Availability Statement

Some or all data, models, or code generated or used during this study are proprietary or confidential in nature and may only be provided with restrictions. For additional information on the profiles used in this study, please consult Kosiba and Wurman (2023).

Acknowledgments

The first author thanks David Bodine at the University of Oklahoma and Anthony Reinhart at the NOAA Cooperative Institute for Severe and High-Impact Weather Research and Operations (CIWRO), David Nolan at the University of Miami, and Nathan Dahl at the Storm Prediction Center (SPC) for access to the numerical simulations. The first and second authors acknowledge funding through the NIST Disaster Resilience and NOAA VORTEX-SE programs for Grant Nos. 70NANB19H057 and NA17OAR4590202, respectively. Input on the development of the tornado profile from members of the ASCE 7 Tornado Task Committee and members of the Radar Subcommittee of the ASCE/AMS Standards Committee for Wind Speed Estimation in Tornadoes and Other Windstorms is gratefully acknowledged.

References

Alexander, C. R., and J. Wurman. 2005. "The 30 May 1998 Spencer, South Dakota, Storm. Part I: The structural evolution and environment of the tornadoes." *Mon. Weather Rev.* 133 (1): 72–97. https://doi.org/10.1175/MWR-2855.1.

ASCE. 2022. *Minimum design loads and associated criteria for buildings and other structures*. ASCE/SEI 7-22. Reston, VA: ASCE.

Ashley, W. S., A. M. Haberlie, and J. Strohm. 2019. "A climatology of quasi-linear convective systems and their hazards in the United States." *Weather Forecasting* 34 (6): 1605–1631. https://doi.org/10.1175/WAF-D-19-0014.1.

Cao, S., M. Wang, and J. Cao. 2018. "Numerical study of wind pressure on low-rise buildings induced by tornado-like flows." *J. Wind Eng. Ind. Aerodyn.* 183 (Dec): 214–222. https://doi.org/10.1016/j.jweia.2018.10.023.

Church, C. R., J. T. Snow, and E. M. Agee. 1977. "Tornado vortex simulation at Purdue University." *Bull. Am. Meteorol. Soc.* 58 (9): 900–908. https://doi.org/10.1175/1520-0477(1977)058<0900:TVSAPU>2.0.CO;2.

Cook, N. J. 1986. *Designers guide to wind loading of building structures. Part 1*. Butterworths, UK: Architectural Press.

Dahl, N. A., D. S. Nolan, G. H. Bryan, and R. Rotunno. 2017. "Using high-resolution simulations to quantify underestimates of tornado intensity from in situ observations." *Mon. Weather Rev.* 145 (5): 1963–1982. https://doi.org/10.1175/MWR-D-16-0346.1.

Davies-Jones, R., R. J. Trapp, and H. B. Bluestein. 2001. "Tornadoes and tornadic storms." In *Severe convective storms*, 167–221. Boston: American Meteorological Society.

FEMA. 2012. "Mitigation assessment team report–Spring 2011 tornadoes: April 25–28 and May 22; Building performance observations, recommendations and technical guidance." Accessed September 16, 2024. https://www.fema.gov/sites/default/files/2020-08/fema_p-908_tornado-mat-combined.pdf.

Gillmeier, S., M. Sterling, H. Hemida, and C. J. Baker. 2018. "A reflection on analytical tornado-like vortex flow field models." *J. Wind Eng. Ind. Aerodyn.* 174 (Mar): 10–27. https://doi.org/10.1016/j.jweia.2017.12.017.

Haan, F. L., Jr., V. K. Balaramudu, and P. P. Sarkar. 2010. "Tornado-induced wind loads on a low-rise building." *J. Struct. Eng.* 136 (1): 106–116. https://doi.org/10.1061/(ASCE)ST.1943-541X.0000093.

Harris, R. I., and D. M. Deaves. 1980. "The structure of strong winds." In *Proc., Wind Engineering in the Eighties: Proc. CIRIA Conf.* London: Construction Industry Research and Information Association.

Hu, H., Z. Yang, P. Sarkar, and F. Haan. 2011. "Characterization of the wind loads and flow fields around a gable-roof building model in tornado-like winds." *Exp. Fluids* 51 (3): 835. https://doi.org/10.1007/s00348-011-1102-6.

Jensen, M. 1958. "The model law phenomena in natural wind." *Ingenioren* 2 (2): 121–128.

Kelly, M., R. A. Cersosimo, and J. Berg. 2019. "A universal wind profile for the inversion-capped neutral atmospheric boundary layer." *Q. J. R. Meteorol. Soc.* 145 (720): 982–992. https://doi.org/10.1002/qj.3472.

Kosiba, K., and J. Wurman. 2010. "The three-dimensional axisymmetric wind field structure of the Spencer, South Dakota, 1998 Tornado." *J. Atmos. Sci.* 67 (9): 3074–3083. https://doi.org/10.1175/2010JAS3416.1.

Kosiba, K., and J. Wurman. 2023. "The strongest winds in tornadoes are very near the ground." *Commun. Earth Environ.* 4 (1): 50. https://doi.org/10.1038/s43247-023-00716-6.

Kosiba, K. A., and J. Wurman. 2013. "The three-dimensional structure and evolution of a tornado boundary layer." *Weather Forecasting* 28 (6): 1552–1561. https://doi.org/10.1175/WAF-D-13-00070.1.

Kuo, H. L. 1971. "Axisymmetric flows in the boundary layer of a maintained vortex." *J. Atmos. Sci.* 28 (1): 20–41. https://doi.org/10.1175/1520-0469(1971)028<0020:AFITBL>2.0.CO;2.

Lee W. C., J. D. Jou, P. L. Chang, and S. M. Deng. 1999. "Tropical cyclone kinematic structure retrieved from single-Doppler radar observations. Part I: Interpretation of Doppler velocity patterns and the GBVTD technique." *Mon. Weather Rev.* 127 (7): 2419–2439. https://doi.org/10.1175/1520-0493(1999)127<2419:TCKSRF>2.0.CO;2.

Lee, W.-C., and J. Wurman. 2005. "Diagnosed three-dimensional axisymmetric structure of the Mulhall Tornado on 3 May 1999." *J. Atmos. Sci.* 62 (7): 2373–2393. https://doi.org/10.1175/JAS3489.1.

Li, Y., B. R. Ellingwood, P. Vickery, S. Banik, and A. M. Salman. 2024. *Reliability bases for Tornado Load Criteria for ASCE Standard 7-22*. Reston, VA: ASCE. https://doi.org/10.1061/JSENDH.STENG-13499.

Lombardo, F. T., D. A. Smith, J. L. Schroeder, and K. C. Mehta. 2014. "Thunderstorm characteristics of importance to wind engineering." *J. Wind Eng. Ind. Aerodyn.* 125 (5): 121–132. https://doi.org/10.1016/j.jweia.2013.12.004.

McAllister, T. P., N. Wang, and B. R. Ellingwood. 2018. "Risk-informed mean recurrence intervals for updated wind maps in ASCE 7-16." *J. Struct. Eng.* 144 (5): 1–4. https://doi.org/10.1061/(ASCE)ST.1943-541X.0002011.

NIST. 2014. *Technical investigation of the May 22, 2011, tornado in Joplin Missouri*. NCSTAR 3. Gaithersburg, MD: NIST.

Nolan, D. S., N. A. Dahl, G. H. Bryan, and R. Rotunno. 2017. "Tornado vortex structure, intensity, and surface wind gusts in large-eddy simulations

with fully developed turbulence." *J. Atmos. Sci.* 74 (5): 1573–1597. https://doi.org/10.1175/JAS-D-16-0258.1.

Refan, M., and H. Hangan. 2016. "Characterization of tornado-like flow fields in a new model scale wind testing chamber." *J. Wind Eng. Ind. Aerodyn.* 151 (Apr): 107–121. https://doi.org/10.1016/j.jweia.2016.02.002.

Refan, M., and H. Hangan. 2018. "Near surface experimental exploration of tornado vortices." *J. Wind Eng. Ind. Aerodyn.* 175 (Apr): 120–135. https://doi.org/10.1016/j.jweia.2018.01.042.

Refan, M., H. Hangan, and J. Wurman. 2014. "Reproducing tornadoes in laboratory using proper scaling." *J. Wind Eng. Ind. Aerodyn.* 135 (Dec): 136–148. https://doi.org/10.1016/j.jweia.2014.10.008.

Refan, M., H. Hangan, J. Wurman, and K. Kosiba. 2017. "Doppler radar-derived wind field of five tornado events with application to engineering simulations." *Eng. Struct.* 148 (Oct): 509–521. https://doi.org/10.1016/j.engstruct.2017.06.068.

Reinhart, A. E., D. J. Bodine, and F. T. Lombardo. 2018. "The impact of terrain on supercells using idealized numerical simulations." In *Proc., 29th Conf. on Severe Local Storms*. Boston: American Meteorological Society.

Tang, Z., C. Feng, L. Wu, D. Zuo, and D. L. James. 2018. "Characteristics of tornado-like vortices simulated in a large-scale ward-type simulator." *Boundary-Layer Meteorol.* 166 (2): 327–350. https://doi.org/10.1007/s10546-017-0305-7.

Wang, J., S. Cao, W. Pang, and J. Cao. 2017. "Experimental study on effects of ground roughness on flow characteristics of tornado-like vortices." *Boundary-Layer Meteorol.* 162 (2): 319–339. https://doi.org/10.1007/s10546-016-0201-6.

Wen, Y. K. 1975. "Dynamic tornado wind loads on tall buildings." *J. Struct. Div.* 101 (1): 169–185. https://doi.org/10.1061/JSDEAG.0003967.

Wood, V. T., and R. A. Brown. 2011. "Simulated tornadic vortex signatures of tornado-like vortices having one-and two-celled structures." *J. Appl. Meteorol. Climatol.* 50 (11): 2338–2342. https://doi.org/10.1175/JAMC-D-11-0118.1.

Wurman, J. 2002. "The multiple-vortex structure of a tornado." *Weather Forecasting* 17 (3): 473–505. https://doi.org/10.1175/1520-0434(2002)017<0473:TMVSOA>2.0.CO;2.

Wurman, J., and K. Kosiba. 2013. "Finescale radar observations of tornado and mesocyclone structures." *Weather Forecasting* 28 (5): 1157–1174. https://doi.org/10.1175/WAF-D-12-00127.1.

Wurman, J., K. Kosiba, T. White, and P. Robinson. 2021a. "Supercell tornadoes are much stronger and wider than damage-based ratings indicate." *PNAS* 118 (14): e2021535118. https://doi.org/10.1073/pnas.2021535118.

Wurman, J., K. A. Kosiba, B. Pereira, P. Robinson, A. Frambach, A. Gilliland, T. White, J. Aikins, R. J. Trapp, and S. Nesbitt. 2021b. "The FARM (flexible array of radars and mesonets)." *Bull. Am. Meteorol. Soc.* 102 (8): E1499–E1525. https://doi.org/10.1175/BAMS-D-20-0285.1.

Wurman, J., K. A. Kosiba, C. Robinson, and T. Marshall. 2014. "The role of multiple vortex tornado structure in causing storm researcher fatalities." *Bull. Am. Meteorol. Soc.* 95 (1): 31–45. https://doi.org/10.1175/BAMS-D-13-00221.1.

Wurman, J., P. Robinson, C. Alexander, and Y. Richardson. 2007. "Low-level winds in tornadoes and potential catastrophic tornado impacts in urban areas." *Bull. Am. Meteorol. Soc.* 88 (1): 31–46. https://doi.org/10.1175/BAMS-88-1-31.

Yeo, D., D. Bott, and B. Lanier. 2023. "ASCE 7-22 wind speed profiles and velocity pressure exposure coefficients for structural design." *J. Struct. Eng.* 149 (5): 04023044. https://doi.org/10.1061/JSENDH.STENG-11370.

Yuan, F., G. Yan, R. Honerkamp, K. M. Isaac, M. Zhao, and X. Mao. 2019. "Numerical simulation of laboratory tornado simulator that can produce translating tornado-like wind flow." *J. Wind Eng. Ind. Aerodyn.* 190 (Jul): 200–217. https://doi.org/10.1016/j.jweia.2019.05.001.

Zhang, W., and P. P. Sarkar. 2012. "Near-ground tornado-like vortex structure resolved by particle image velocimetry (PIV)." *Exp. Fluids* 52 (2): 479–493. https://doi.org/10.1007/s00348-011-1229-5.